Full-wavelet approach for fluorescence diffuse optical tomography with structured illumination

Nicolas Ducros,[1,*] Cosimo D'andrea,[1,2] Gianluca Valentini,[1,2] Tim Rudge,[3] Simon Arridge,[3] and Andrea Bassi[1]

[1]*Instituto di Fotonica e Nanotecnologie (IFN-CNR)—Dipartimento di Fisica, Politecnico di Milano, Piazza Leonardo da Vinci 32, I-20133 Milan, Italy*

[2]*Italian Institute of Technology (IIT), Piazza Leonardo da Vinci 32, I-20133 Milan, Italy*

[3]*Centre for Medical Image Computing, University College London, Malet Place, London WC1E 6BT, UK*

**Corresponding author: nicolas.ducros@polimi.it*

Received July 30, 2010; revised September 14, 2010; accepted September 29, 2010; posted October 4, 2010 (Doc. ID 132612); published October 28, 2010

We present a fast reconstruction method for fluorescence optical tomography with structured illumination. Our approach is based on the exploitation of the wavelet transform of the measurements acquired after wavelet-patterned illuminations. This method, validated on experimental data, enables us to significantly reduce the acquisition and computation times with respect to the classical scanning approach. Therefore, it could be particularly suited for *in vivo* applications. © 2010 Optical Society of America

OCIS codes: 170.6960, 170.7050, 100.7410, 100.3190.

Diffuse optical tomography (DOT) is usually considered in terms of measurements acquired by a set of point detectors and illuminated by a set of point sources. However, the modality is now evolving toward the use of spatially extended sources and detectors. Recently, spatial light modulators and wide-field detectors have been exploited for both absorption and fluorescence reconstructions. In particular, digital micromirror devices (DMDs), able to project any pattern of light onto a sample, have been involved in imaging [1] and tomographic schemes [2–5]. Fast algorithms able to deal with very large datasets have been proposed for this modality [6,7], and it was observed that a limited number of patterns can be used in contrast to a large number of point-source illuminations. In parallel, the concept of data compression based on Fourier [8] or wavelet encoding [9,10] has been recently applied to CCD measurements acquired with point sources, in order to reduce the computational size of the problem.

In this Letter, for the first time to our knowledge, we apply compression techniques to the measurements acquired with structured illuminations, implementing a simple approach that relies on the wavelet description of both source and detection spaces. This approach is experimentally validated in the context of fluorescence DOT (FDOT), regarding a solid phantom containing two fluorescent inclusions. The success of wavelet algorithms for a large number of applications in biomedical imaging mainly lies in the compression properties of wavelet bases [11]. Here, they are used (1) as a guide to design sets of a few illumination patterns and (2) to reduce the redundancy in the measurements. Limiting the number of illumination patterns directly reduces acquisition times. Limiting both the number of illumination patterns and features extracted from the CCD measurements reduces the size of the inverse problem to solve, which speeds up the reconstruction times.

We consider a domain Ω with boundary ∂D and a light source that illuminates a part $\partial S \subset \partial D$ of the surface. The medium contains a fluorophore concentration $c(\mathbf{r})$, $\mathbf{r} \in \Omega$, and the fluorescence light emitted from the surface ∂D is recorded by a camera. Practically, structured illumination in FDOT consists of four steps: (1) projection of the source pattern on ∂S, (2) collection of the fluorescence light ϕ^m on ∂D, (3) transformation of the raw data, and (4) reconstruction of the concentration $c(\mathbf{r})$ from the transformed data m. Discretizing the medium Ω into N voxels leads to the discrete linear problem

$$\mathbf{m} = \mathbf{W}\mathbf{c}, \tag{1}$$

where $\mathbf{c}$ is the concentration vector, $\mathbf{m}$ is the measurement vector, and $\mathbf{W}$ is the weight matrix.

Let us define the set of functions $\mathcal{S} = \{s_j\}$, $j = 1 \ldots J$, describing the *source patterns* projected on ∂S. For a given source pattern s_j, the physics of the problem obey the coupled equations [12]

$$\begin{cases} \mathcal{P}\phi_j^x(\mathbf{r}) = s_j(\mathbf{r}), \\ \mathcal{P}\phi_j^m(\mathbf{r}) = \phi_j^x(\mathbf{r})c(\mathbf{r})\mathrm{d}\mathbf{r}, \end{cases} \tag{2}$$

where appropriate boundary conditions must be taken into account to complete the description. In Eqs. (2), $\mathcal{P}$ denotes the propagation operator, and ϕ_j^x and ϕ_j^m are the photon densities at the excitation and emission wavelengths, respectively.

Let us now consider a set of functions $\mathcal{D} = \{d_{j,k}\}$, $j = 1 \ldots J$, $k = 1 \ldots K$, defined on ∂D and referred to as *detection patterns*. Note that the detection patterns can vary from source pattern to source pattern. Then, we define the measurements as the projections of the fluorescence photon densities ϕ_j^m onto the detection patterns, i.e., for a given source–detection pattern pair:

$$m_{j,k} = \int_{\partial D} \phi_j^m(\mathbf{r}) d_{j,k}(\mathbf{r})\mathrm{d}\mathbf{r}. \tag{3}$$

In practice, the source patterns s_j and the measured fluorescence density ϕ_j^m are images that can be represented using a wavelet basis. The wavelet transform

(WT) of an image at scale s is obtained by projecting this image onto an appropriate set of functions $\{a^s, b^s\}$. The set of scaling functions $\{a^s\}$ provides a multiresolution approximation of the space function, i.e., approximated versions of an image at higher resolutions for increasing scale s. The set of wavelet functions $\{b^s\}$ provides the complementary details that are not comprised in the approximated image. Here, the source patterns are chosen as the wavelet scaling functions at a given scale, while the detection patterns are determined by performing the WT of the fluorescence images.

The detailed scheme of our full-wavelet algorithm is the following.

Step 1. *Illumination/Acquisition*: at scale s, J wavelet source patterns $\mathbf{s}_j$ are computed and successively projected onto the medium. The resulting J fluorescence light images ϕ_j^m are acquired.

Step 2. *Compression*: the fluorescence light image ϕ_j^m is wavelet transformed and the K largest absolute components in the transformed image are retained. The corresponding K wavelet functions form the set of the detection patterns associated to the jth source pattern, which is noted $\mathcal{D}_j$. Applying this procedure to the J fluorescence light images ends up with a measurement vector $\mathbf{m}$ of size JK. The whole set of detection patterns is $\mathcal{D} = \bigcup_j \mathcal{D}_j$, whose number of elements is at most JK, but can be reduced to J due to redundancy in the detection patterns.

Step 3. *Weight matrix computation*: the weight matrix $\mathbf{W}$ of size $(JK \times N)$ is computed from the knowledge of the source and detection patterns. Indeed, the (j,k)th row of $\mathbf{W}$, which maps $\mathbf{c}$ onto $m_{j,k}$, is the product of a direct and an adjoint field computation given by

$$\mathbf{w}_{j,k} = (\varphi_j \circ \psi_{j,k})^T, \tag{4}$$

where $\circ$ stands for the entrywise (Hadamard) product. The source and detection photon density vectors φ_j and $\psi_{j,k}$ are taken from the matrices $\mathbf{\Phi} = [\varphi_1 \ldots \varphi_j \ldots \varphi_J]$ and $\mathbf{\Psi} = [\psi_{1,1} \ldots \psi_{j,k} \ldots \psi_{J,K}]$ obtained by inverting the two systems

$$\mathbf{P\Phi} = \mathbf{S}, \tag{5a}$$

$$\mathbf{P\Psi} = \mathbf{D}. \tag{5b}$$

In Eq. (5), $\mathbf{S} = [\mathbf{s}_1 \ldots \mathbf{s}_j \ldots \mathbf{s}_J]$ is the source matrix, $\mathbf{D} = [\mathbf{d}_{1,1} \ldots \mathbf{d}_{j,k} \ldots \mathbf{d}_{J,K}]$ is the detection matrix, and $\mathbf{P}$ results from the discretization of the propagation operator $\mathcal{P}$ accounting for the boundary conditions. Here, the propagation matrix $\mathbf{P}$ was calculated by solving the diffusion approximation equation with the finite-element TOAST package [13].

Step 4. *Inversion*: as an estimate of the concentration vector, the underdetermined Tikhonov regularized solution $\mathbf{c}^*$ is considered, i.e.,

$$\mathbf{c}^* = \mathbf{W}^T(\mathbf{W}\mathbf{W}^T + \alpha\mathbf{I})^{-1}\,\mathbf{m}, \tag{6}$$

where α is the regularization parameter. In the following, α was set to 10^{-5} tr $\mathbf{W}\mathbf{W}^T$.

The method is validated experimentally on an epoxy phantom chosen to mimic the size and optical properties of a small animal. The light generated (625 nm, 500 mW) by an LED (M625L2, Thorlabs, USA) is bandpass filtered (XF1208, Omega, USA) and projected on a DMD (DMD Discovery 1100, Vialux, Germany). The desired source pattern is uploaded on the DMD and projected onto the phantom [3]. The fluorescence light is bandpass filtered (XF3076, Omega, USA) and collected by an objective lens ($f = 50$ mm, f-number $= 2.8$, Nikon Co., Japan). It is then integrated for 30 s by a 16 bit CCD camera (Versarray 512, Princeton Instruments, Trenton, N.J.) cooled to −40 °C. A parallelepiped phantom of size 32 mm × 64 mm × 15 mm, absorption coefficient $\mu_a = 0.012\ \text{mm}^{-1}$, reduced scattering coefficient $\mu_s' = 0.827\ \text{mm}^{-1}$, and refractive index $n = 1.54$ is considered. Two cylindrical chambers (diameter 3 mm and length 3 mm) were drilled into the phantom. The first one is centered at position $\mathbf{r_1} = [17, 20, 3]$ mm and the second one at position $\mathbf{r_2} = [20, 40, 8]$ mm. The two chambers are each filled with 21 μL of Nyle Blue in water solution at 34 μM.

We first investigate the compression ability of different WTs for the acquired fluorescence images [14]. In Fig. 1, we consider the fluorescence image acquired for a uniform source pattern [see Fig. 1(a)]. Applying different kinds of WTs and retaining only 16 coefficients indicates the compression performance on this image [Fig. 1(b)]. The Battle–Lemarié functions achieve compression of fluorescence images with the least degradation of those tested. This is therefore the basis considered in the following, as also used in [9].

Next, we perform three-dimensional (3-D) reconstructions according to the scheme previously described. The simulated data have been corrupted by a Poisson noise model assuming an integration time giving a maximum

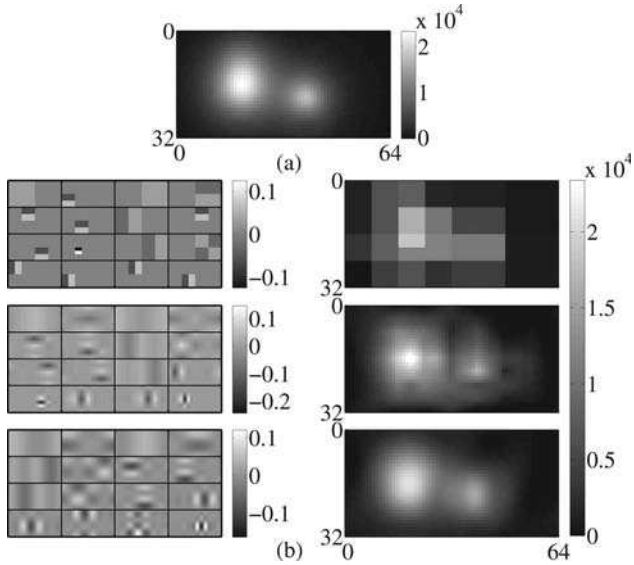

Fig. 1. Wavelet compression of fluorescence images. (a) Fluorescence image acquired with a uniform source pattern. (b) From top to bottom, Haar, Daubechie, and Battle–Lemarié wavelets are considered. On the left, we display the 16 retained wavelet patterns. On the right, the compressed version of the upper image is depicted.

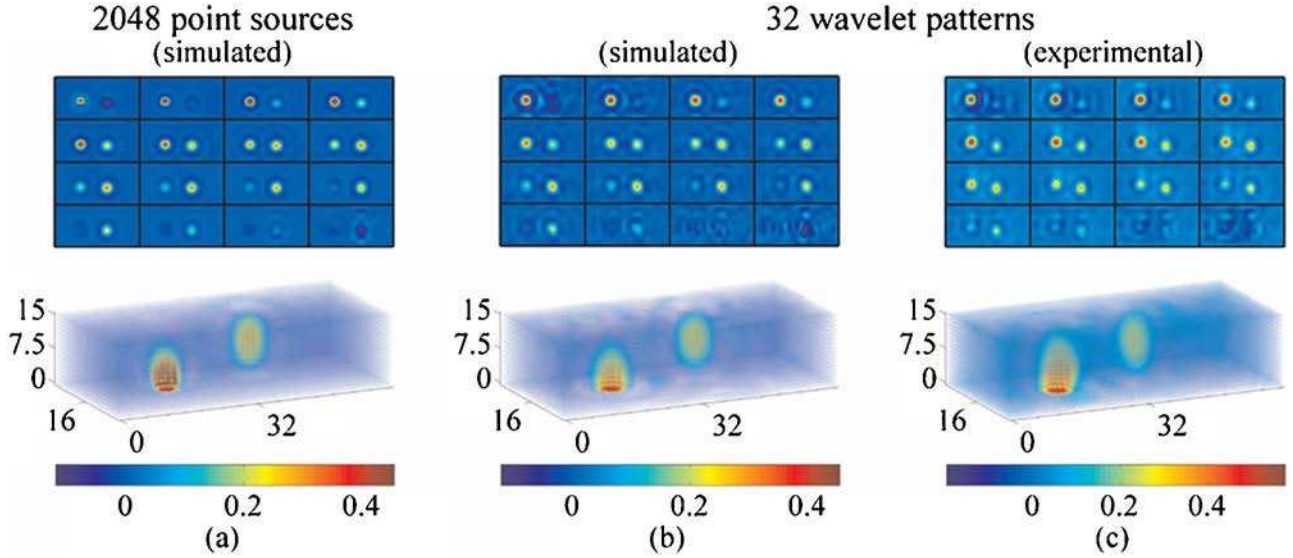

Fig. 2. (Color online) Reconstruction for different source patterns. The fluorescence images have been compressed to 24 Battle–Lemarié wavelet coefficients. (a) Standard scanning approach using 2048 sources positions (simulated); $\epsilon = 0.58$. (b) Wavelet approach using 32 patterns (simulated); $\epsilon = 0.70$. (c) Wavelet approach using 32 patterns (experimental); $\epsilon = 0.99$.

of 4000 counts. In Fig. 2, we present reconstruction obtained from a scanning acquisition with 1 mm spacing [Fig. 2(a)] and reconstructions obtained from the projection of a limited number of wavelet source patterns [Figs. 2(b) and 2(c)]. As a quantitative evaluation of the different reconstruction qualities, we estimate the reconstruction error $\epsilon = \|\mathbf{c}_{\text{true}} - \mathbf{c}^*\|^2/\|\mathbf{c}_{\text{true}}\|^2$ and report its value in Fig. 2. The computation times of the reconstructions are detailed in Table 1. When the 2048 point sources are considered, the total reconstruction time is about 18 min, while less than 10 s are required considering the 32 wavelet patterns. As can be observed on the sections at different depths and on the 3-D plots of Fig. 2, the bottom inclusion is less resolved when the 32 wavelet patterns are considered. However, the reconstruction quality obtained with the wavelet approach is comparable to that resulting from the raster scanning. Moreover, the reconstruction performed from experimental data is very close to that obtained from the simulated data.

In conclusion, we have introduced and demonstrated on experimental data a fast algorithm for structured illumination in FDOT. Our approach consists of illuminating the medium with only a few wavelet patterns and compressing the acquired images by means of a wavelet transform. Compared to the classical raster scanning method, the proposed approach enables us to drastically reduce both acquisition and reconstruction times without sacrificing the reconstruction quality. Hence this approach could be relevant for *in vivo* applications for which time is a critical point. In further work, we will apply this approach to the cylindrical geometry and show how it compares to the state of the art.

Table 1. Computation Times (s) of the Reconstructions Presented in Fig. 2[a]

	Step 2		Step 3				Step 4
	$\mathbf{m}$	$\mathcal{D}$	$\mathbf{P}$	Φ	Ψ	$\mathbf{W}$	$\mathbf{c}^*$
Point	5	3	0.8	95	25	60	876
Wavelet	0.1	<0.1	0.8	3.4	3.4	0.8	0.5

[a] $\mathbf{m}$, time for wavelet transform of all acquired image data; $\mathcal{D}$, time for generation of wavelet source patterns; $\mathbf{P}$, time for construction of propagation matrix; Φ, solve time for all source photon densities [Eq. (5a)]; Ψ, solve time for all detection photon densities [Eq. (5b)]; $\mathbf{W}$, construction of weight matrix [Eq. (4)]; $\mathbf{c}^*$, solve time for reconstruction [Eq. (6)].

This work was supported in part by the Royal Society International Joint Project 2009/R2 and the CARIPLO Foundation (grant 2009-2626).

References

1. D. J. Cuccia, F. Bevilacqua, A. J. Durkin, and B. J. Tromberg, Opt. Lett. **30**, 1354 (2005).
2. A. Joshi, W. Bangerth, and E. M. Sevick-Muraca, Opt. Express **14**, 6516 (2006).
3. A. Bassi, C. D'Andrea, G. Valentini, R. Cubeddu, and S. Arridge, Opt. Lett. **34**, 2156 (2009).
4. S. Bélanger, M. Abran, X. Intes, C. Casanova, and F. Lesage, J. Biomed. Opt. **15**, 016006 (2010).
5. C. D'Andrea, N. Ducros, A. Bassi, S. Arridge, and G. Valentini, Biomed. Opt. Express **1**, 106 (2010).
6. V. Lukic, V. A. Markel, and J. C. Schotland, Opt. Lett. **34**, 983 (2009).
7. S. D. Konecky, A. Mazhar, D. Cuccia, A. J. Durkin, J. C. Schotland, and B. J. Tromberg, Opt. Express **17**, 14780 (2009).
8. J. Ripoll, Opt. Lett. **35**, 688 (2010).
9. T. J. Rudge, V. Y. Soloviev, and S. R. Arridge, Opt. Lett. **35**, 763 (2010).
10. N. Ducros, A. D. Silva, J.-M. Dinten, C. S. Seelamantula, M. Unser, and F. Peyrin, Med. Phys. **37**, 2890 (2010).
11. M. Unser and A. Aldroubi, Proc. IEEE **84**, 626 (1996).
12. S. R. Arridge and J. C. Schotland, Inverse Probl. **25**, 123010 (2009).
13. M. Schweiger and S. R. Arridge, TOAST package, http://web4.cs.ucl.ac.uk/research/vis/toast/ (2010).
14. D. Donoho, A. Maleki, and M. Shahram, Wavelab 850, http://www-stat.stanford.edu/~wavelab/ (2010).